NANO LETTERS

pubs.acs.org/NanoLett
Letter

Deep Learning Assisted Plasmonic Dark-Field Microscopy for Super-Resolution Label-Free Imaging

Ming Lei, Junxiang Zhao, Ayse Z. Sahan, Jie Hu, Junxiao Zhou, Hongki Lee, Qianyi Wu, Jin Zhang, and Zhaowei Liu*

Cite This: https://doi.org/10.1021/acs.nanolett.4c04399

ABSTRACT: Dark-field microscopy (DFM) is a widely used imaging tool, due to its high-contrast capability in imaging label-free specimens. Traditional DFM requires optical alignment to block the oblique illumination, and the resolution is diffraction-limited to the wavelength scale. In this work, we present deep-learning assisted plasmonic dark-field microscopy (DAPD), which is a single-frame super-resolution method using plasmonic dark-field (PDF) microscopy and deep-learning assisted image reconstruction. Specifically, we fabricated a designed PDF substrate with surface plasmon polaritons (SPPs) illuminating specimens on the substrate. Dark field images formed by scattered light from the specimen are further processed by a pretrained convolutional neural network (CNN) using a simulation dataset based on the designed substrate and parameters of the detection optics. We demonstrated a resolution enhancement of 2.8 times on various label-free objects with a large potential for future improvement. We highlight our technique as a compact alternative to traditional DFM with a significantly enhanced spatial resolution.

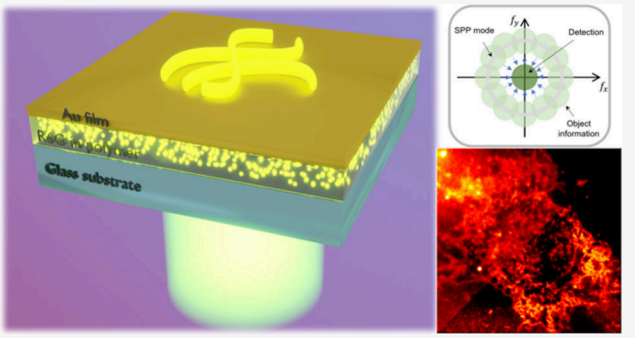

KEYWORDS: *Super resolution, dark field microscopy, surface plasmon polaritons, deep learning*

Optical microscopy has been an indispensable tool for biological and chemical studies since its first invention in the 17th century. In the realm of microscopy, the pursuit of finer resolutions and higher contrasts has been a constant endeavor. However, Abbe's diffraction limit had long confined microscopy to a fundamental resolution threshold. In the past few decades, the emergence of super resolution microscopy technologies such as stimulated emission depletion (STED) microscopy, stochastic optical reconstruction microscopy (STORM), photoactivated localization microscopy (PALM) and structured illumination microscopy (SIM), enables scientists to delve into previously invisible realms of the nanoscale world.[1−4] While these methods provide excellent spatial resolution, they all rely on fluorescent labels, which are prone to photobleaching and suffer other difficulties associated with the usage of fluorophores.[5−7]

Label-free imaging allows for the direct observation of samples in their native states, preserving their natural characteristics and dynamic behaviors.[8] However, it is often limited by low contrast between the specimen and the surrounding refractive indices, as well as by diffraction-limited spatial resolution. Traditional label-free imaging techniques, such as dark-field microscopy, phase-contrast microscopy, and differential interference contrast microscopy, improve image contrast compared to bright-field imaging but still suffer from limited resolution.[9−13] In recent years, several novel techniques in the label-free imaging domain have been developed.[14−17] Interferometric scattering microscopy (iSCAT) was introduced to detect nanometer-scale objects with high sensitivity and contrast by leveraging the interference between scattered light from the object and reflected illumination.[18] However, its resolution remains diffraction limited. Fourier ptychographic microscopy (FPM), based on the synthetic aperture concept, achieves resolution improvement using a light-emitting diode (LED) array as the illumination source.[19] Tens of images are recorded under LEDs from different illuminating angles and used for super-resolution image reconstruction in both amplitude and phase. Despite its advantages, FPM requires a complex optical setup and numerous subframes for image reconstruction, limiting its imaging speed.

In recent years, the field of optical imaging has been significantly impacted by deep learning (DL), yielding remarkable achievements in addressing intricate inverse

Received: September 9, 2024
Revised: November 21, 2024
Accepted: November 22, 2024

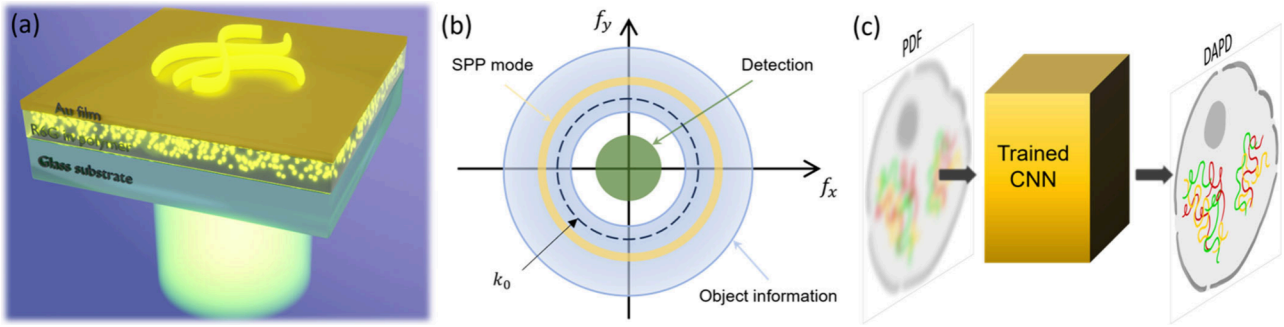

Figure 1. Schematic of DAPD working principle. (a) DAPD substrate schematic. Laser projected on the substrate excites the fluorescent emission layer (R6G in PMMA). R6G emission light is coupled into SPP mode at the top gold surface. Specimen atop of the Au film is illuminated by the SPPs. The scattered light is detected by an objective and forms a dark field image. (b) Fourier space relationship between the SPP illumination light, free space k-vector (k_0), diffraction-limit detection range, and the actual information collected from the object. (c) Super-resolution DAPD image could be reconstructed by a pretrained CNN with a single-frame low-resolution PDF image as input.

problems.[20−26] In contrast to traditional reconstruction approaches that typically necessitate explicit mathematical models to derive analytical solutions, DL neural networks rely on extensive datasets to autonomously learn and tackle complex inverse quandaries. Well-designed neural networks have been effectively employed in numerous super-resolution imaging techniques.[27−30] For instance, deep-STORM makes use of a fully convolutional encoder−decoder network trained on simulation dataset to achieve comparable resolution in STORM with higher emitter density and reconstruction speed.[31] Rationalized deep learning super-resolution microscopy was developed to increase the resolution in low signal-to-noise (SNR) ratio structure illumination microscopy image reconstruction.[32] These neural networks thereby enhance the capabilities of prevailing imaging methods, in terms of either speed or resolution.

In this work, we propose and experimentally demonstrate a new label-free super-resolution imaging method termed deep-learning assisted plasmonic dark-field microscopy (DAPD) that offers a 2.8-fold improvement in spatial resolution. In DAPD, a designed plasmonic substrate is used to generate SPPs with a large wave vector as dark-field illumination. SPPs scattered by the specimen on the substrate become far-field detectable and form diffraction-limited dark-field images which contain high k information on the object. The diffraction-limited plasmonic dark-field images are further processed by a pretrained neural network into super-resolution dark-field images. The neural network is trained on a simulation data set generated based on the designed substrate and detection optics. The performance of the framework is evaluated on both simulated and experimental images including transparent beads and COS-7 cells, which demonstrate a resolution improvement of ∼2.8 times. Requiring only a single-frame diffraction-limited image for reconstruction, DAPD is also capable of high-speed imaging. The proposed technique has the potential to become a significant tool in biomedical and chemical research with its compact architecture and super-resolution capability in label-free imaging.

In traditional DFM, oblique dark-field illumination light is generated with a dark-field ring and cannot enter the objective lens. The objective only collects a scattered beam from the object to form a background-free image. As a result, the illumination wave vector in the object plane is slightly bigger than the detection numerical aperture (NA) but always smaller than k_0, which is the free space wave vector of the illumination light. It has been demonstrated that, with the oblique illumination in DFM, the high spatial frequency information encoded in the diffraction-limited image can be retrieved with deep learning neural networks.[33] The resolution improvement was restricted to 2-fold, due to the limitation of the wave vector of illumination light.

To overcome such a limit, we designed a plasmonic dark-field substrate to provide a high-k illumination source. As shown in Figure 1a, the DAPD substrate consists of 2 layers, including a light emission layer and a SPP mode supporting layer. The light emission layer (200 nm thick) is composed of a transparent polymer mixed with fluorescent dye. The excited fluorescent dyes in the polymer will be directly coupled into the SPP mode of the gold film at the emission wavelength with SPP k-vectors in every possible planar direction.[34] The coupled SPP on gold film serves as illumination, which can be collected by the objective only when scattered by the specimen within the evanescent wave range. As a result, the background remains dark in the acquired image, which makes it a dark-field image.[34] Importantly, with plasmonic dark-field substrate, the illumination wave vector is determined by the k-vector of the SPP mode which is always larger than free space k_0. Since no SPP waves can be directly detected in the far field, this illumination scheme assures a clean dark-field background, regardless of the objective used in detection. In addition, the SPP k-vector can be designed with values much higher than those accessible in traditional dark-field microscopes. More details about the plasmonic substrate design can be found in Figure S1.

In DAPD, higher spatial frequency information is encoded in diffraction-limited images. In a similar manner to the synthetic aperture method, the high-k illumination SPP shifts high spatial frequency information on the object into the limited detection bandwidth. As shown in Figure 1b, the SPP mode in Fourier space is a ring with higher k-vectors than both the objective detection range and the free-space k_0. The object information that is detected and encoded in the diffraction limited dark-field image is a donut in Fourier space, as illustrated in Figure 1b. The relationship between the illumination, imaging system detection, and detected object information in the Fourier space can be mathematically written as

$$O_d(k_x, k_y) = I_{SPP}(k_x, k_y) \otimes H(k_x, k_y) \quad (1)$$

https://doi.org/10.1021/acs.nanolett.4c04399
Nano Lett. XXXX, XXX, XXX−XXX

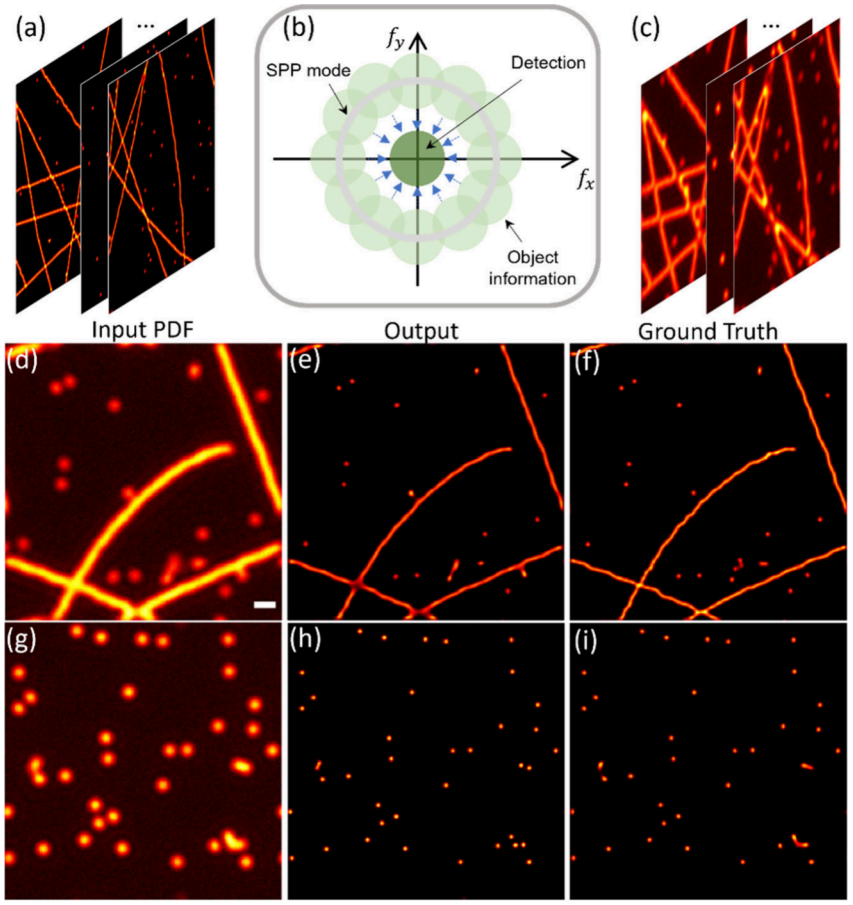

Figure 2. Simulation method for dataset generation and reconstruction performance. (a) Generated ground truth super-resolution images with random objects. (b) Fourier space manipulation of ground truth information. SPP mode illumination shifts the high-k information on the object into detection band to form the diffraction-limited PDF image in panel (c). (d, g) Simulated low-resolution PDF images of edges and scattering particles for network performance test. (e, h) Network output super-resolution DAPD images. (f, j) Object ground truth. Scale bar = 1 μm.

where O_d is the Fourier spectrum of detected object information, I_{SPP} the Fourier spectrum of the illumination SPP mode, and H the coherent transfer function of the imaging system. Therefore, the effective numerical aperture (NA_{eff}) of the imaging is defined as $NA_{eff} = NA_{obj} + NA_{SPP}$, where NA_{obj} is the numerical aperture of the objective and NA_{SPP} is the numerical aperture of the illumination SPP mode. As a result, the DAPD raw image contains much higher resolution information on the object than the normal dark-field image.

Once the raw plasmonic dark-field image is acquired from the object, an image processing tool is necessary to extract the high-k information encoded in the low-resolution image. Retrieving the high-resolution image is extremely challenging, because all the high-k information produced from the high-k SPP illumination is concentrated and encoded in a single diffraction-limited image frame, making it an ill-posed problem, which is difficult to solve with mathematical equations or optimization techniques. Convolutional neural networks (CNNs) have gained significant attention in the optical imaging field due to their excellent performance in complex image processing tasks, including super-resolution, denoising, and image segmentation.[35−37] In this work, we use a pretrained CNN to process the low-resolution plasmonic dark-field image and generate a super-resolution output.

Collecting a sufficient image dataset is crucial for ensuring the quality of network training. However, this process can be very time-consuming for many imaging technologies. In super-resolution microscopy, obtaining ground truth images is particularly challenging. In this work, given that the forward imaging model is known, we employ a simulation method to estimate the low-resolution plasmonic dark-field image of any given object based on the design of the plasmonic substrate and imaging system, which is shown in Figures 2a−c. In DAPD, the SPP mode on the Au film illuminates the specimen, and the scattered beam is detected by the imaging system. Due to the incoherent fluorescent illumination, the PDF image can be calculated as a superposition of images under each SPP mode. With a given object, the low-resolution PDF image can be estimated as

$$I_{PDF} = \sum_{i=1}^{m} |F^{-1}[U(k + k_{spp,i})\cdot H(k)]|^2 + n \quad (2)$$

where U is the Fourier spectrum of the object spatial information, H is the coherent transfer function of the imaging system, $k_{spp,i}$ is the k-vector of the SPP mode at different directions, m is the total number of SPP modes, and n is the additive white Gaussian noise (signal-to-noise (S/N) ratio = 35). The final PDF image is calculated by summarizing the image intensity produced from different SPP mode illumination. The simulation image dataset is numerically generated and processed using MATLAB R2020b. As shown in Figure 2b, the estimation is more accurate with a larger m. In practice, we use m = 30 to balance the simulation performance and

https://doi.org/10.1021/acs.nanolett.4c04399
Nano Lett. XXXX, XXX, XXX−XXX

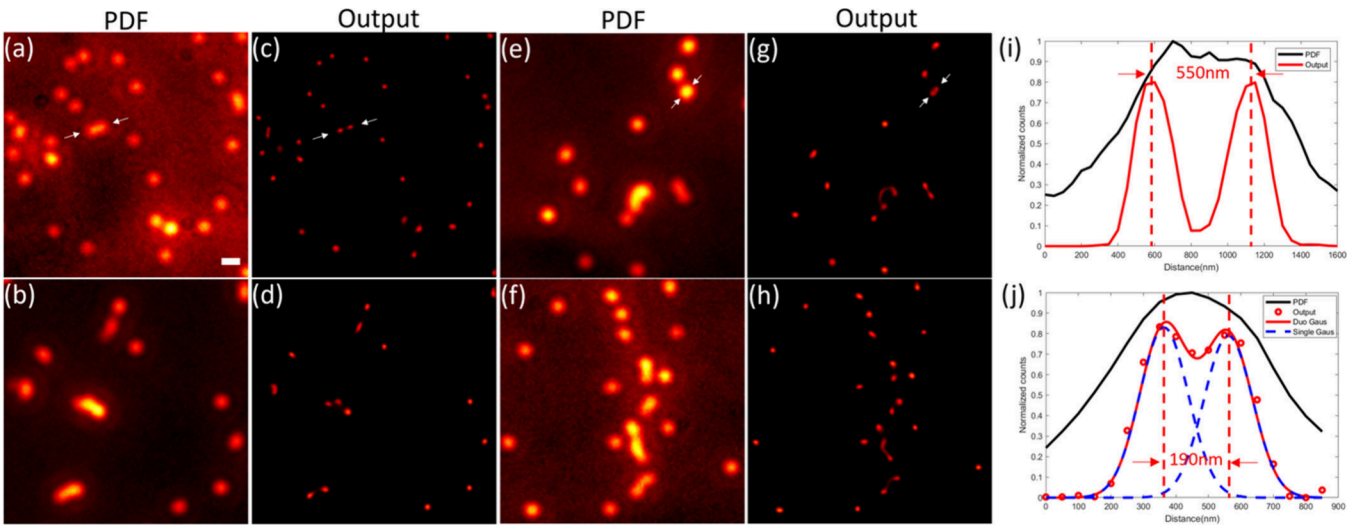

Figure 3. Experimental demonstration of DAPD by using 200 nm polystyrene beads. (a, b, e, f) Low-resolution PDF image before neural network processing. (c, d, g, h) Super-resolution DAPD reconstructed images. (i) Cross-section profile of the object marked with a pair of arrows line in panels (a) and (c). (j) Cross-section profile of the object marked with a pair of arrows line in panels (e) and (g). Dark line represents the original low-resolution PDF image. Red circles represent the output image pixels. Red solid line represents the fitted curve of two Gaussian functions and the blue dashed lines display the single Gaussian curve from each bead. Scale bar = 1 μm.

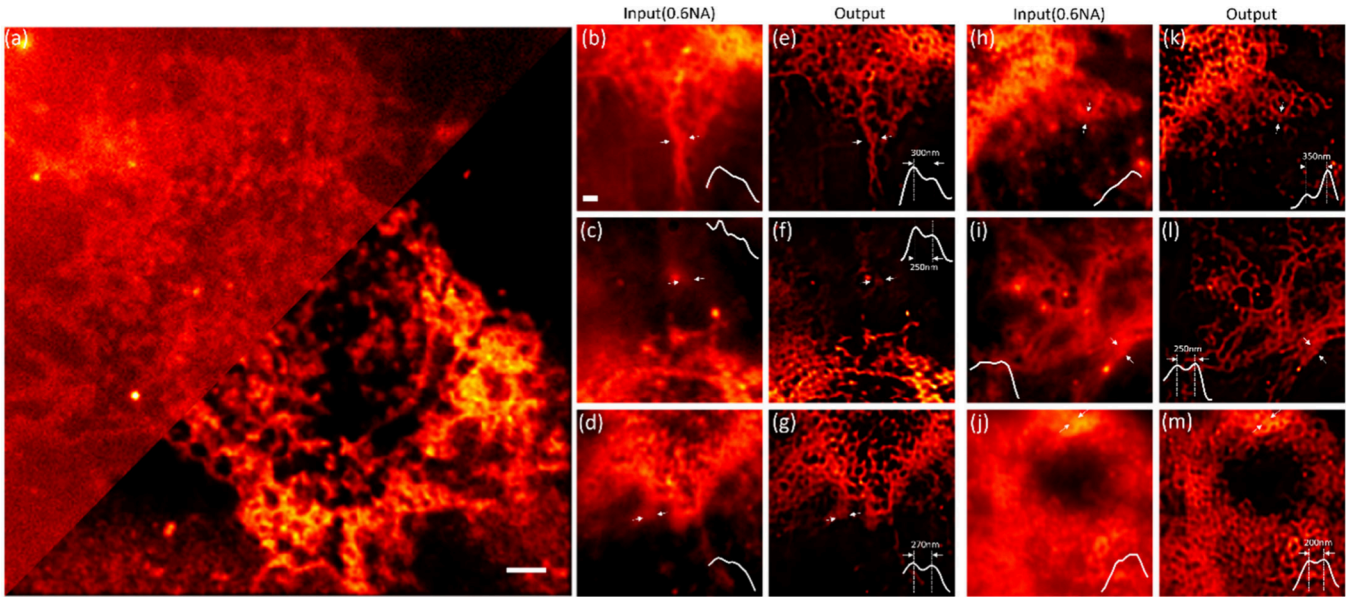

Figure 4. Trained network performance on experiment data with cells. (a) PDF image of single COS-7 cell. Top-left is the diffraction-limit PDF image, and bottom-right is the network processed DAPD image. (b–d, h–j) Diffraction-limited PDF images acquired with a 40×/0.6NA objective. (e–g, k–m) DAPD super-resolved images. Scale bar = 2 μm in panel (a) and 1 μm in all other panels. All the cross-section profiles are magnified twice for better visualization.

computation cost. More information about the effective optical transfer function and choice of m can be found in Figure S2.

The simulated training dataset is then used to train a U-net structure for super-resolution reconstruction. More information about the network structure and loss function can be found in Figure S3. The training and testing processes are executed on a desktop computer equipped with a NVIDIA GeForce GTX2070S graphic cards and a Core i7−9700K CPU @ 3.6 GHz. 3000 pairs of simulated images are used for training and the batch size is set to be 15. Input images are cropped to be 256 × 256 in size. After training with the simulation dataset, we test the network performance with previously unseen simulation images. As shown in Figures 2d−i, the diffraction limited PDF images are successfully reconstructed to a super-resolution dark-field image of the object. We use structure and similarity index measure (SSIM) and peak signal-to-noise ratio (PSNR) to compare the network output and object ground truth to evaluate the reconstructed images, which shows a SSIM of 0.9885 ± 0.008 and a PSNR of 33.049 ± 0.019 dB.

To fabricate the DAPD substrate for experiments, we cleaned coverslips with acetone under sonication for 10 min, followed by rinsing with isopropanol and deionized water. R6G powder (Thermo Fisher) were dissolved in PMMA 495A4 solution in anisole (MicroChem). The solution was then filtered with a 0.22 μm membrane filter (Millex Express) three

https://doi.org/10.1021/acs.nanolett.4c04399
Nano Lett. XXXX, XXX, XXX−XXX

times, followed by centrifuge under 17g for 1 h to further remove the impurities. The purified R6G-PMMA solution was then spin-coated on coverslips under 3000 rpm for 1 min. The substrate was placed on a 150 °C hot plate for 7 min to form a 200 nm film. After the PMMA is annealed, 40 nm Au film was deposited on the substrate using E-beam evaporation before the DAPD substrates were ready for use.

With the fabricated DAPD substrates, we demonstrated the success of the trained neural network in different samples. Initially, we demonstrated the resolution improvement of DAPD by imaging polystyrene beads (Invitrogen, USA) 200 nm in diameter. The beads were diluted 10 times and drop-cast on DAPD substrates before imaging. The substrate was imaged under an inverted microscope (Model IX83, Olympus). We used a 532 nm laser guided by a multimode fiber as illumination to excite the Rhodamine 6G (R6G) in poly(methyl methacrylate) (PMMA). The multimode fiber was attached to a rotating eccentric motor to remove the speckle in illumination. The scattering signal was then collected by a 40×/0.6NA objective lens, followed by a 4× magnification before the camera. Considering $k_{spp} \approx 1.1k_0$, we have $NA_{eff} \approx 1.7$ for the DAPD microscopy. A 532-nm notch filter (Semrock) and a 20-nm bandpass filter centered at 588 nm (Semrock) were used to block the laser transmission. The images shown in Figure 3 were recorded with a CCD camera (iXon 897, Andor) and processed by a trained neural network. The low-resolution image was expected to have a resolution of ∼500 nm. The network output images in Figures 3c−h show that the polystyrene beads with ∼200 nm diameters can be clearly resolved. As shown in Figure 3j, double Gaussian fitting was applied to the high-resolution output image of the beads and shows a 190-nm center-to-center distance, which corresponds to an ∼2.8 times resolution improvement and matches the theoretical estimation.

Subsequently, we imaged COS-7 cells using the same microscope setup as that previously described. COS-7 cells used in this study were acquired from ATCC and were cultured in Dulbecco's modified Eagle medium (DMEM) (Gibco, Lot No. 11995-065) including 4.5 g/L glucose, 4 mM L-glutamine, 1.5 g/L sodium bicarbonate, and 1 mM sodium pyruvate, supplemented with 10% fetal bovine serum (FBS) (Gibco, Lot No. 26140-079), and 1% (v/v) penicillin/streptomycin (Pen/Strep) (Gibco, Lot No. 15140−122). Cells were routinely tested for mycoplasma contamination and found to be negative. For experiments, cells were plated onto DAPD substrate 24 h prior to imaging.

Although the network had not encountered COS-7 cells during the training process, it still achieved commendable reconstruction results. The images presented in Figures 4b−d and 4h−j illustrate the unprocessed plasmonic dark-field (PDF) images of COS-7 cells, which appear blurred due to the diffraction limit. In contrast, the network's output, shown in Figures 4e−g and 4k−m, clearly resolves cellular features close to the surface of the substrate, with structures as small as 200 nm being distinctly identifiable. Additional data, including Fourier spectrum comparisons and Fourier ring correlation results, are provided in Figure S5. To illustrate the resolution enhancement achieved by DAPD, we also compared the DAPD reconstruction results with those obtained using the Lucy−Richardson deconvolution algorithm, as presented in Figure S6.

The resolution enhancement in this study is attributed to the high-k illumination of the SPP mode on the Au surface. For a gold−air interface, $k_{spp} \approx 1.1k_0$ has been demonstrated to increase the resolution limit beyond that of traditional dark-field microscopy. The fluorescent emission from dye molecules within the near field of the Au film is coupled to the SPP mode. Although the 40-nm Au film blocks a significant portion of the fluorescent emission in other directions, some transmitted fluorescent signals remain, serving as background noise in the raw plasmonic dark-field image. In the meantime, the surface roughness of the plasmonic substrate caused by the polymer spin-coating and Au film deposition also introduces additional background noise from scattering of the SPP mode. Consequently, the scattering cross-section of the object must be sufficiently large to ensure the visibility. The 2.8-fold resolution improvement demonstrated in this work allows for the resolution of features down to 200 nm, which can still be considered strong scatterers compared to the 527-nm wavelength of SPP on Au.

The SPP mode excitation is achieved by coupling fluorescent emission to the near field. Note that the lifetime of the DAPD substrate is limited due to the photobleaching effect of the fluorescent dye. In this study, we used a saturated solution of R6G to maximize the lifetime of the substrate under laser excitation. In the future, substrates can be further improved by using electroluminescence layer like GaAs or GaN p−n junction to excite SPPs on the metal film.[38] This will not only extend the lifetime of the substrate but also reduce the cost of optical setup since the illumination laser is no longer needed, making super-resolution dark-field microscopy more accessible. The resolution in DAPD is primarily determined by the numerical aperture of the detection objective and the k-vector of the SPP mode. In fact, the effective numerical aperture of the imaging system is the combination of an illumination k-vector and the detection k-vector. Resolution can be further enhanced by using a substrate that supports SPP with higher k-vector.[39−41] It is important to emphasize that the improvement in resolution is also constrained by the design and implementation of neural networks. To achieve substantial advancements in resolution, the development of new network architectures that are more effectively tailored to focus on high-k information is still required. See Figure S4 for more information.

DAPD microscopy is primarily suited for surface imaging because the SPP mode exhibits an evanescent exponential decay with distance from the substrate. Scatterers within the evanescent range are enhanced by SPP illumination, resulting in high-contrast dark-field images. This makes DAPD microscopy particularly useful for observing structures near the surface. However, for thicker objects with greater spatial distribution away from the surface, the scattering signal weakens, reducing the imaging effectiveness.

In summary, we have proposed and demonstrated DAPD microscopy, a label-free super-resolution imaging technique. This method leverages near-field high-k illumination of SPP waves and spatial frequency unmixing of the object information. High spatial frequency information is encoded by the high-k SPP illumination and detected in low-resolution plasmonic dark-field images. These images are then processed by a pretrained neural network to reconstruct high-resolution images. By replacing traditional dark-field microscope illumination optics with a specially designed plasmonic substrate, we also reduce the complexity of the optical setup. Compared with the diffraction limit, DAPD microscopy shows a 2.8-fold resolution improvement on different specimens with single-

https://doi.org/10.1021/acs.nanolett.4c04399
Nano Lett. XXXX, XXX, XXX−XXX

frame detection. This technique holds significant potential for numerous label-free super-resolution imaging applications.

■ ASSOCIATED CONTENT

Data Availability Statement

Data and codes underlying this work may be obtained from the corresponding author upon reasonable request.

Supporting Information

The Supporting Information is available free of charge at https://pubs.acs.org/doi/10.1021/acs.nanolett.4c04399.

Plasmonic dark-field substrate design (Figure S1); illumination approximation in dataset simulation (Figure S2); neural network architecture (Figure S3); discussion of limit of the resolution improvement (Figure S4); Fourier spectrum and resolution analysis (Figure S5); DAPD reconstruction comparison with deconvolution (Figure S6) (PDF)

■ AUTHOR INFORMATION

Corresponding Author

Zhaowei Liu − *Department of Electrical and Computer Engineering and Materials Science and Engineering, University of California−San Diego, La Jolla, California 92093, United States;* orcid.org/0000-0002-5732-8109; Email: zhaowei@ucsd.edu

Authors

Ming Lei − *Department of Electrical and Computer Engineering, University of California−San Diego, La Jolla, California 92093, United States;* orcid.org/0000-0001-6687-9044

Junxiang Zhao − *Department of Electrical and Computer Engineering, University of California−San Diego, La Jolla, California 92093, United States*

Ayse Z. Sahan − *Department of Pharmacology, University of California−San Diego, La Jolla, California 92093, United States; Biomedical Sciences Graduate Program, University of California, San Diego, California 92093, United States*

Jie Hu − *Department of Electrical and Computer Engineering, University of California−San Diego, La Jolla, California 92093, United States*

Junxiao Zhou − *Department of Electrical and Computer Engineering, University of California−San Diego, La Jolla, California 92093, United States;* orcid.org/0000-0001-6168-8580

Hongki Lee − *Department of Electrical and Computer Engineering, University of California−San Diego, La Jolla, California 92093, United States;* orcid.org/0000-0002-0655-1925

Qianyi Wu − *Department of Electrical and Computer Engineering, University of California−San Diego, La Jolla, California 92093, United States;* orcid.org/0000-0001-8060-2340

Jin Zhang − *Department of Pharmacology and Shu Chien − Gene Lay Department of Bioengineering, University of California−San Diego, La Jolla, California 92093, United States; Department of Chemistry and Biochemistry, University of California, San Diego, California 92093, United States*

Complete contact information is available at: https://pubs.acs.org/10.1021/acs.nanolett.4c04399

Notes

The authors declare no competing financial interest.

■ ACKNOWLEDGMENTS

This work was supported by the NSF Biophotonics program, under Grant No. 2348536 (to Z.L.), and NIH Grant No. R35 CA197622 (to J.Z.).

■ REFERENCES

(1) Willig, K. I.; Rizzoli, S. O.; Westphal, V.; Jahn, R.; Hell, S. W. STED microscopy reveals that synaptotagmin remains clustered after synaptic vesicle exocytosis. *Nature* **2006**, *440*, 935−939.

(2) Rust, M. J.; Bates, M.; Zhuang, X. Sub-diffraction-limit imaging by stochastic optical reconstruction microscopy (STORM). *Nat. Meth.* **2006**, *3*, 793−796.

(3) Betzig, E.; et al. Imaging intracellular fluorescent proteins at nanometer resolution. *Science* **2006**, *313*, 1642−1645.

(4) Gustafsson, M. G. Surpassing the lateral resolution limit by a factor of two using structured illumination microscopy. *J. Microsc.* **2000**, *198*, 82−87.

(5) Huang, B.; Bates, M.; Zhuang, X. Super-resolution fluorescence microscopy. *Annu. Rev. Biochem.* **2009**, *78*, 993−1016.

(6) Lichtman, J. W.; Conchello, J.-A. Fluorescence microscopy. *Nat. Meth.* **2005**, *2*, 910−919.

(7) Leung, B. O.; Chou, K. C. Review of super-resolution fluorescence microscopy for biology. *Appl. Spectrosc.* **2011**, *65*, 967−980.

(8) Silva, W. R.; Graefe, C. T.; Frontiera, R. R. Toward label-free super-resolution microscopy. *ACS Photonics* **2016**, *3*, 79−86.

(9) Gao, P. F.; Lei, G.; Huang, C. Z. Dark-field microscopy: recent advances in accurate analysis and emerging applications. *Anal. Chem.* **2021**, *93*, 4707−4726.

(10) Burch, C.; Stock, J. Phase-contrast microscopy. *J. Sci. Instrum.* **1942**, *19*, 71.

(11) Pluta, M. Nomarski's DIC Microscopy: A Review. In *Phase Contrast Differential Interference Contrast Imaging Techniques Applications*; Pluta, M., Szyjer, M., Eds., Nomarski's DIC microscopy: a review. Phase contrast differential interference contrast imaging techniques applications; Proceedings of SPIE, Vol. *1846*; SPIE, 1994; pp 10−25.

(12) Ueno, H.; et al. Simple dark-field microscopy with nanometer spatial precision and microsecond temporal resolution. *Biophys. J.* **2010**, *98*, 2014−2023.

(13) Horio, T.; Hotani, H. Visualization of the dynamic instability of individual microtubules by dark-field microscopy. *Nature* **1986**, *321*, 605−607.

(14) Wu, Q.; et al. Single-shot quantitative amplitude and phase imaging based on a pair of all-dielectric metasurfaces. *Optica* **2023**, *10*, 619−625.

(15) Mazumder, N.; Balla, N. K.; Zhuo, G.-Y.; Kistenev, Y. V.; Kumar, R.; Kao, F.-J.; Brasselet, S.; Nikolaev, V. V.; Krivova, N. A.; et al. Label-free non-linear multimodal optical microscopy—basics, development, and applications. *Front. Phys.* **2019**, *7*, 170.

(16) Vicar, T.; Balvan, J.; Jaros, J.; Jug, F.; Kolar, R.; Masarik, M.; Gumulec, J.; et al. Cell segmentation methods for label-free contrast microscopy: review and comprehensive comparison. *BMC Bioinform.* **2019**, *20*, 1−25.

(17) Liu, J.; et al. Intrinsic optical spatial differentiation enabled quantum dark-field microscopy. *Phys. Rev. Lett.* **2022**, *128*, 193601.

(18) Ortega-Arroyo, J.; Kukura, P. Interferometric scattering microscopy (iSCAT): new frontiers in ultrafast and ultrasensitive optical microscopy. *Phys. Chem. Chem. Phys.* **2012**, *14*, 15625−15636.

(19) Zheng, G.; Horstmeyer, R.; Yang, C. Wide-field, high-resolution Fourier ptychographic microscopy. *Nat. Photonics* **2013**, *7*, 739−745.

(20) Rivenson, Y.; et al. Deep learning microscopy. *Optica* **2017**, *4*, 1437−1443.

(21) Zhang, H.; et al. High-throughput, high-resolution deep learning microscopy based on registration-free generative adversarial network. *Biomed. Opt. Express* **2019**, *10*, 1044−1063.
(22) Barbastathis, G.; Ozcan, A.; Situ, G. On the use of deep learning for computational imaging. *Optica* **2019**, *6*, 921−943.
(23) Suzuki, K. Overview of deep learning in medical imaging. *Radiol. Phys. Technol.* **2017**, *10*, 257−273.
(24) Razzak, M. I.; Naz, S.; Zaib, A. Deep learning for medical image processing: Overview, challenges and the future. In *Classification in BioApps: Automation of Decision Making*, 2018; pp 323−350 DOI: 10.1007/978-3-319-65981-7_12.
(25) Hughes, L. H.; Merkle, N.; Bürgmann, T.; Auer, S.; Schmitt, M. In *IGARSS 2019—2019 IEEE International Geoscience and Remote Sensing Symposium*; IEEE, 2019; pp 4877−4880.
(26) Midtvedt, B.; Helgadottir, S.; Argun, A.; Pineda, J.; Midtvedt, D.; Volpe, G. Quantitative digital microscopy with deep learning. *Appl. Phys. Rev.* **2021**, *8*, 011310.
(27) Cheng, Y. F.; et al. Illumination pattern design with deep learning for single-shot Fourier ptychographic microscopy. *Opt. Express* **2019**, *27*, 644−656.
(28) Yang, W.; et al. Deep learning for single image super-resolution: A brief review. *IEEE Trans. Multimedia* **2019**, *21*, 3106−3121.
(29) Qiao, C.; et al. Evaluation and development of deep neural networks for image super-resolution in optical microscopy. *Nat. Meth.* **2021**, *18*, 194−202.
(30) Park, H.; Na, M.; Kim, B.; Park, S.; Kim, K. H.; Chang, S.; Ye, J. C.; et al. Deep learning enables reference-free isotropic super-resolution for volumetric fluorescence microscopy. *Nat. Commun.* **2022**, *13*, 3297.
(31) Nehme, E.; Weiss, L. E.; Michaeli, T.; Shechtman, Y. Deep-STORM: super-resolution single-molecule microscopy by deep learning. *Optica* **2018**, *5*, 458−464.
(32) Qiao, C.; et al. Rationalized deep learning super-resolution microscopy for sustained live imaging of rapid subcellular processes. *Nat. Biotechnol.* **2023**, *41*, 367−377.
(33) Lei, M.; Zhao, J.; Zhou, J.; Lee, H.; Wu, Q.; Burns, Z.; Chen, G.; Liu, Z. Super resolution label-free dark-field microscopy by deep learning. *Nanoscale* **2024**, *16*, 4703.
(34) Hu, H.; Ma, C.; Liu, Z. Plasmonic dark field microscopy. *Appl. Phys. Lett.* **2010**, *96*, 113107.
(35) Yamanaka, J.; Kuwashima, S.; Kurita, T. In *.Neural Information Processing: 24th International Conference, ICONIP 2017, Proceedings, Part II 24*, Guangzhou, China, Nov. 14−18, 2017; Springer, 2017, pp 217−225.
(36) Zhang, K.; Zuo, W.; Zhang, L. FFDNet: Toward a fast and flexible solution for CNN-based image denoising. *IEEE Trans. Image Process.* **2018**, *27*, 4608−4622.
(37) Minaee, S.; Boykov, Y. Y.; Porikli, F.; Plaza, A. J; Kehtarnavaz, N.; Terzopoulos, D.; et al. Image segmentation using deep learning: A survey. *IEEE Trans. Pattern Analysis Machine Intell.* **2021**, *44*, 3523−3542.
(38) Wei, F.; Wan O, Y.; Li, G.; Cheah, K. W.; Liu, Z. Organic light-emitting-diode-based plasmonic dark-field microscopy. *Opt. Lett.* **2012**, *37*, 4359−4361.
(39) Ferrari, L.; Wu, C.; Lepage, D.; Zhang, X.; Liu, Z. Hyperbolic metamaterials and their applications. *Progress Quantum Electron.* **2015**, *40*, 1−40.
(40) Yanik, A. A.; et al. Seeing protein monolayers with naked eye through plasmonic Fano resonances. *Proc. Natl. Acad. Sci. U.S.A.* **2011**, *108*, 11784−11789.
(41) Zentgraf, T.; Liu, Y.; Mikkelsen, M. H.; Valentine, J.; Zhang, X. Plasmonic Luneburg and Eaton Lenses. *Nat. Nanotechnol.* **2011**, *6*, 151−155.

https://doi.org/10.1021/acs.nanolett.4c04399
Nano Lett. XXXX, XXX, XXX−XXX